1521-0103/382/3/356–365$35.00
THE JOURNAL OF PHARMACOLOGY AND EXPERIMENTAL THERAPEUTICS
dx.doi.org/10.1124/jpet.122.001284
J Pharmacol Exp Ther 382:356–365, September 2022

The Journal of PHARMACOLOGY And Experimental Therapeutics

Intratracheal Administration of Acyl Coenzyme A Acyltransferase-1 Inhibitor K-604 Reduces Pulmonary Inflammation Following Bleomycin-Induced Lung Injury[S]

Emily R. Stevenson, Melissa L. Wilkinson, Elena Abramova, Changjiang Guo, and Andrew J. Gow

Ernest Mario School of Pharmacy, Department of Pharmacology & Toxicology, Rutgers, The State University of New Jersey, Piscataway, New Jersey

Received April 22, 2022; accepted June 28, 2022

ABSTRACT

Acute lung injury (ALI) is characterized by epithelial damage, barrier dysfunction, and pulmonary edema. Macrophage activation and failure to resolve play a role in ALI; thus, macrophage phenotype modulation is a rational target for therapeutic intervention. Large, lipid-laden macrophages have been observed in various injury models, including intratracheal bleomycin (ITB), suggesting that lipid storage may play a role in ALI severity. The endoplasmic reticulum-associated enzyme acyl coenzyme A acyltransferase-1 (Acat-1/*Soat1*) is highly expressed in macrophages, where it catalyzes the esterification of cholesterol, leading to intracellular lipid accumulation. We hypothesize that inhibition of Acat-1 will reduce macrophage activation and improve outcomes of lung injury in ITB. K-604, a selective inhibitor of Acat-1, was used to reduce cholesterol esterification and hence lipid accumulation in response to ITB. Male and female C57BL6/J mice (n = 16-21/group) were administered control, control + K-604, ITB, or ITB + K-604 on d0, control or K-604 on d3, and were sacrificed on day 7. ITB caused significant body weight loss and an increase in cholesterol accumulation in bronchoalveolar lavage cells. These changes were mitigated by Acat-1 inhibition. K-604 also significantly reduced ITB-induced alveolar thickening. Surfactant composition was normalized as indicated by a significant decrease in phospholipid: SP-B ratio in ITB+K-604 compared with ITB. K-604 administration preserved mature alveolar macrophages, decreased activation in response to ITB, and decreased the percentage mature and pro-fibrotic interstitial macrophages. These results show that inhibition of Acat-1 in the lung is associated with reduced inflammatory response to ITB-mediated lung injury.

SIGNIFICANCE STATEMENT

Acyl coenzyme A acyltransferase-1 (Acat-1) is critical to lipid droplet formation, and thus inhibition of Acat-1 presents as a pharmacological target. Intratracheal administration of K-604, an Acat-1 inhibitor, reduces intracellular cholesterol ester accumulation in lung macrophages, attenuates inflammation and macrophage activation, and normalizes mediators of surface-active function after intratracheal bleomycin administration in a rodent model. The data presented within suggest that inhibition of Acat-1 in the lung improves acute lung injury outcomes.

1. Introduction

Acute lung injury (ALI) affects approximately 200,000 people in the United States annually and has a high mortality rate due to respiratory failure (Johnson and Matthay, 2010; Dushianthan et al., 2011). ALI is characterized by inflammation, resulting in changes to innate immune cell, endothelial, and epithelial cell function (Matthay and Zimmerman, 2005; Johnson and Matthay, 2010). These alterations present as diffuse alveolar damage, epithelial and endothelial barrier dysfunction (Tam et al., 2011; Müller-Redetzky et al., 2014), pulmonary edema (Butt et al., 2016), and surfactant dysfunction (Cross and Matthay, 2011; Mokra and Kosutova, 2015; Butt et al., 2016). The primary management strategy for patients is mechanical ventilation (Johnson and Matthay, 2010; Dushianthan et al., 2011; Patel et al., 2018), which can lead to worse patient outcomes due to ventilation-perfusion mismatch, further tissue damage due to barotrauma, and altered inflammatory responses (Ioannidis et al., 2015). Therefore, identifying an effective pharmacological treatment is advantageous for this patient population.

Macrophage-mediated inflammation is a critical component in the pathogenesis of ALI (Huang et al., 2018; Chen et al., 2020). As the first line of defense for innate immune responses

This work was supported by the National Institutes of Health National Heart, Lung, and Blood Institute [Grant R01-HL086621] (to A.J.G.) and the National Institutes of Health National Institute of Environmental Health Sciences [Grant T32-ES01984] and [Grant P30-ES005022].
No author has an actual or perceived conflict of interest with the contents of this article.
dx.doi.org/10.1124/jpet.122.001284.
[S] This article has supplemental material available at jpet.aspetjournals.org.

ABBREVIATIONS: Acat-1, acyl coenzyme A acyltransferase-1; ALI, acute lung injury; A.U., arbitrary unit; Arg1, inducible arginase; BAL, bronchoalveolar lavage; ITB, intratracheal bleomycin; LXR, liver X receptor; *Nos2*, inducible nitric oxide synthase; SP-B, sterol O-acyltransferase-1; SP-D, surfactant protein D.

(Hussell and Bell, 2014; Hartl et al., 2018), macrophages play a crucial role in detecting foreign toxicants, particulates, and pathogens, initiating a cascade of host defenses (Martin and Frevert, 2005; Hartl et al., 2018). Macrophages are highly plastic (Hussell and Bell, 2014) and can be stimulated to express a spectrum of phenotypes that contribute to both inflammation and injury resolution in the lung (Porcheray et al., 2005; Benoit et al., 2008; Laskin, 2009; Johnston et al., 2012; Laskin et al., 2019). Early in the pathogenesis of ALI, alveolar macrophages release pro-inflammatory cytokines (Patel et al., 2018; Chen et al., 2020), attracting neutrophils to the site of injury (Cortés et al., 2012; Patel et al., 2017). Macrophages responsible for the generation of reactive oxygen and nitrogen species may contribute to the majority of the cellular injury observed in ALI (Pittet et al., 1997; Ware, 2006). These chemical species damage the alveolar epithelium and endothelium, promoting increased permeability in the lung, leading to edema and proteinaceous debris accumulation in the alveoli (Cortés et al., 2012; Butt et al., 2016). When this signaling is aberrant or overly persistent, the macrophage response may promote further injury rather than transition to resolution (Laskin et al., 2019). Therefore, regulating macrophage activation presents as a logical target when considering intervention in ALI.

In addition to ALI, macrophages have been implicated in driving the atherosclerotic process (Yu et al., 2013). Excess accumulation of lipids in macrophages drives their activation and progression toward atherosclerotic plaque formation, contributing to vascular injury (Yu et al., 2013; Chistiakov et al., 2016). Research into the mechanisms of foam cell formation led to the discovery of acyl coenzyme Acholesterol acyltransferase-1 (Acat-1/*Soat1*) (Chang et al., 1993; Chang et al., 2001; Chang et al., 2009). Acat-1 catalyzes the conversion of cholesterol to cholesterol esters, a process essential for lipid droplet formation (Chang et al., 2001; Chang et al., 2009). As such, the persistence of lipid-laden cells is critically dependent upon cholesterol esterification (Sekiya et al., 2011; Yu et al., 2013; Chistiakov et al., 2017). These lipid-laden cells exhibit a 'foamy' appearance and have been implicated as a driving force in atherosclerosis (Ross, 1999; Stöger et al., 2012; Yang et al., 2020). Therefore, altering macrophage phenotype in the context of atherosclerotic plaques has been a topic of investigation for some time (Chinetti-Gbaguidi et al., 2015; Bouhlel et al., 2007; Yang et al., 2020); prior research in this area may also have utility in the management of pulmonary pathologies.

As lipid-laden macrophages have been observed in animal models of ALI (Venosa et al., 2019), we propose that inhibition of Acat-1 in the lung will lead to a reduction in injury. Studies varying the route of administration of Acat-1 inhibitors led to the hypothesis that the intratracheal administration of K-604 could effectively target pulmonary cells, mitigate lipid accumulation, modulate cell phenotype, and reduce disease severity in a model of ALI. To test this hypothesis, we have used the intratracheal bleomycin (ITB)-induced model of ALI (Chen et al., 2001; Genovese et al., 2005; Wilkinson et al., 2020) and the novel intratracheal administration of K-604. We found that K-604 administration reduced ALI severity, altered pulmonary cell cholesterol ester formation, and altered alveolar and interstitial macrophage phenotype. These data suggest that Acat-1 inhibition in the lung reduces the inflammatory response to ITB-mediated injury.

2. Materials and Methods

2.1 Animal Use. Six- to 8-week-old male and female wild-type C57BL6/J mice obtained from Jackson Laboratories (Bar Harbor, ME, USA) were used for all experiments. Mice were housed under standard conditions in groups of four per cage with food and water provided ad libitum. All experiments were conducted in accordance with Rutgers University Institutional Animal Care and Use Committee-approved protocols adhering to the U.S. National Institutes of Health Guide for the Care and Use of Laboratory Animals.

2.1. 1 ITB and K-604 Administration. Mice were anesthetized with isoflurane and received a single intratracheal instillation of either 50 μl of PBS (6% DMSO, control), 50 μl of 10 mg/kg K-604 in PBS (6% DMSO) (Sigma Aldrich, St. Louis, MO, Cat No. SML1837) (K-604), 50 μl of 3 U/kg bleomycin in 6% DMSO (Santa Cruz Biotechnology, Inc., Dallas, TX, Cat No. sc-200134B) (ITB), or 10 mg/kg of K-604 + 3 U/kg bleomycin (ITB + K-604), at a total volume of 50 μ with 6% DMSO (Gaylord Chemical Company, L.L.C., Tuscaloosa, AL) as previously described (Guo et al., 2016; Wilkinson et al., 2020; Golden et al., 2022). Mice were observed to ensure the full dose was administered and mice recovered from anesthesia. Seventy-two hours later, mice were re-anesthetized and intratracheally administered 50 μl of PBS or 10 mg/kg K-604 (150 μl, 6% DMSO) (Guo et al., 2016; Wilkinson et al., 2020; Golden et al., 2022). Mice were sacrificed 7 days post intratracheal administration of K-604 or bleomycin. Mice were euthanized via a single intraperitoneal injection of ketamine (135 mg/kg) and xylazine (30 mg/kg) (Fort Dodge Animal Health, Fort Dodge, IA). Absence of pedal reflex was noted before exposing the chest cavity, and a thoracotomy was performed. Lungs were perfused with PBS via cardiac perfusion.

2.2 Bronchoalveolar Lavage (BAL) and Phospholipid Analysis. BAL fluid was collected by instilling 5 × 1 ml of ice cold PBS through a 20-gauge canula inserted into the trachea. BAL fluid was centrifuged at 300 × g for 8 minutes, and the supernatant was assessed for protein concentration using a Pierce BCA Protein Assay (Thermo Scientific, Rockford, IL). Large and small aggregate fractions of BAL were separated from the large aggregate fraction according to the methods of Bligh and Dyer (Bligh and Dyer, 1959). Phospholipid analysis was adapted from the method of Bartlett (Bartlett, 1959). Samples of equal phospholipid content were loaded onto Bis(2-hydroxyethyl)-imino-tris(hydroxymethyl)-methane gels (4–12%, ThermoFisher Scientific, Rockford, IL), transferred to polyvinylidene fluoride membranes, and blocked in non-fat dried milk (10% with 5% Tris-Tween buffered saline) to prevent non-specific binding. Membranes were incubated overnight with either surfactant protein D (SP-D, Duke University, Durham, NC) and SP-B (University of Pennsylvania, Philadelphia, PA) primary antibody and were incubated with Goat-anti-Rabbit horseradish peroxidase (Bio-Rad Cat No. 170-6515) before visualization with ECL Prime Western Blotting Detection Reagent (Amersham Biosciences, Amersham, UK, Cat No. RPN2232). BAL cell pellets were resuspended in 1 ml of staining buffer (5% FBS in 1x PBS, 0.2% sodium azide) and assessed for viability using Trypan Blue Solution (0.4%, ThermoFisher Scientific, Rockford, IL).

2.3 BAL Cell Cholesterol Measurement. 10,000 to 20,000 cells were reserved from the BAL fluid to determine the concentration of total cholesterol, free cholesterol, and cholesterol esters in BAL cell samples. A bioluminescent Cholesterol/Cholesterol Ester-Glo Assay (Promega, Madison, WI) was used, and luminescence was recorded on a SpectraMaxM2 multi-mode microplate reader (Molecular Devices, San Jose, CA) utilizing SoftMax Pro software v5.3.

2.4 Histology Preparation and Analysis. After BAL fluid collection, the large left lung lobe was excised and inflation fixed in paraformaldehyde (3%) and embedded in paraffin. Four-micrometer sections were stained with hematoxylin and eosin to observe histologic changes. Slides were scanned at 40x using a VS120 Virtual Slide Microscope (Olympus, Waltham, MA) and viewed with OlyVIA viewing software for virtual slide images (Olympus, Waltham, MA) at 400x. Randomly selected areas (n = 10) from each histologic slide were

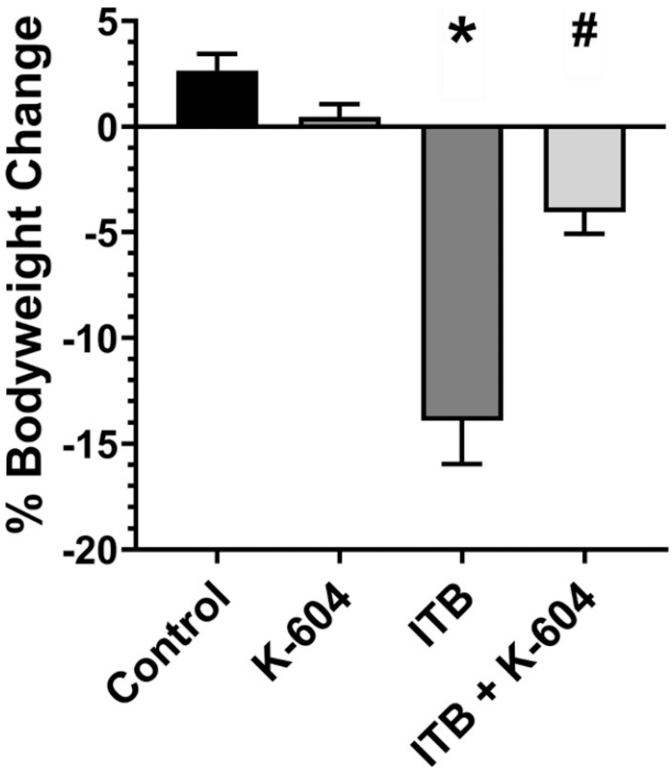

Fig. 1. Intratracheal administration of K-604 reduces ITB-mediated loss of bodyweight. Difference between d0 and d7 bodyweight is shown as a percentage of d0 weight (n = 16–21 per group). Values are expressed as mean ± standard error of the mean. (*) represents significantly different from control ($P < 0.05$); (#) represents significantly different from ITB ($P < 0.05$).

captured and analyzed by a blinded observer to determine average alveolar wall thickness, cell infiltration (# of nuclei), and tissue consolidation (% open tissue space) using ImageJ (NIH).

2.5 Lung Tissue Digestion and CD45+ Cell Separation. After BAL collection, lung tissue was cut into small pieces and digested in 5 ml of 2 mg/ml collagenase type IV (Sigma Aldrich, St. Louis, MO) in RPMI 1640 1x (ThermoFisher Scientific, Rockford, IL) and 5% FBS (ThermoFisher Scientific, Rockford, IL). Tissue was filtered through a 70-μm strainer and washed with RPMI/5% FBS until the strainer was absent of tissue. The filtrate was centrifuged for 6 minutes at 400 × g, and supernatant was aspirated. The remaining cell pellet was resuspended in 1 ml of Red Blood Cell Lysis Buffer (Sigma Aldrich, St. Louis, MO) for 5 minutes at room temperature. Five milliliters of RPMI/5% FBS was added, and cells were centrifuged again for 6 minutes at 400 × g. Supernatant was aspirated, and the cell pellet was counted and resuspended at a concentration of 1×10^8 in 2% FBS in 1x PBS/1 mM EDTA. Immunomagnetic selection of CD45+ leukocytes was performed using the EasySep Mouse CD45 Positive Selection Kit (Stemcell Technologies, Cambridge, MA). CD45+ selected cells and flowthrough (assumed CD45- cells) were recovered. Cells were then stained and processed for flow cytometry.

2.6 Flow Cytometry. Cells from the BAL or lung tissue digest were brought up to a volume of 100 μl of staining buffer. To prevent non-specific binding in the staining and analysis, cells were incubated with TruStain FcX anti-mouse CD16/32 (Fc Block, 1:100) (Biolegend, San Diego, CA, Cat No. 101320) for 10 minutes at 4°C. Samples from the BAL and CD45+ cells from the lung digest were incubated for 30 minutes at 4°C in a cocktail of the following antibodies (1:100): CD11b (BioLegend, San Diego, CA, Cat No. 101206), CD206 (BioLegend, San Diego, CA, Cat No. 141706), F4/80 (BioLegend, San Diego, CA, Cat No. 123114), CD11c (BioLegend, San Diego, CA, Cat No. 117312), CD45 (BioLegend, San Diego, CA, Cat No. 103128), Ly6c (B&D Biosciences, San Diego, CA, Cat No. 562728), Siglec F (BD Biosciences, Franklin Lakes, NJ, Cat No. 565528), and MHC II (Invitrogen, Waltham, MA, Cat No. 48-5321-82). Cells were centrifuged for 6 minutes at 400 × g and washed with staining buffer. Cells were stained with eFluor 780-conjugated fixable viability dye (Invitrogen, Waltham, MA, Cat No. 65-0865-14) for 30 minutes at 4°C, washed with staining buffer, and fixed in 3% paraformaldehyde. Cells were analyzed using a Gallios 10-color flow cytometer (Beckman Coulter, Brea, CA). Using Kaluza software (Beckman Coulter, Brea, CA), cells were initially sorted based upon forward and side scatter, doublet discrimination, and viability (Supplemental Fig. 1, Supplemental Fig. 2) and further analyzed to determined discrete cell phenotypes.

2.7 Reverse-Transcription Polymerase Chain Reaction. BAL macrophages recovered from each group were preserved in 1 ml of TRIzol Reagent (ThermoFisher Scientific, Rockford, IL). In brief, RNA was extracted using phenol-chloroform. After a 15-minute centrifugation at 14,000 × g, the aqueous phase was removed, and RNA was extracted with isopropanol and spun at 14,000 × g. The pellet was isolated and washed with 70% ethanol, dried, and resuspended in 15 μl of RNase-free ultrapure water. After heating at 70°C for 10 minutes, RNA was quantitated using a NanoDrop 1000 spectrophotometer (ThermoFisher Scientific, Rockford, IL) and stored. cDNA was prepared according to a High-Capacity cDNA Reverse Transcription Kit (ThermoFisher Scientific, Rockford, IL) with a final target concentration of 200 ng/μl. Taqman assays were used to analyze relative gene expression using Taqman fast master mix (Thermofisher Scientific, Rockford, IL) and the following Taqman primers: G*apdh* (Mm99999915_g1), *Nos2* (Mm00440502_m1), *Arg1* (Mm00475988_m1), A*bca1* (Mm00442646_m1), and A*bcg1* (Mm00437390_m1). A threshold of 40 cycles was used as the limit of detection for gene expression. Thermal cycle numbers greater than 40 were set to 40 cycles for the purpose of the analysis. ΔΔct values were calculated using *Gapdh* as the control gene and PBS as the control condition. Fold change was calculated as $2^{(-\Delta\Delta ct)}$.

2.8 Statistical Analysis. Statistical analysis was performed using GraphPad Prism Software version 9.0.2 for Windows (GraphPad Software, San Diego, CA). Quantitative data were analyzed by two-way ANOVA. Multiple comparisons were followed by Holm-Sidak test with a significance level of $P < 0.05$ compared with control (*) and ITB ($^{\#}$). Data are shown as mean ± standard error of the mean.

3. Results

3.1 K-604 Mitigates ALI and Improves ITB-Induced Histologic Changes. ITB administration resulted in a decreased body weight compared with controls in alignment with previously conducted studies (Barbayianni et al., 2018). On average, ITB mice lost 14 ± 2.1% body weight over 7 days, which was significantly blunted to a loss of 4±1.0%$^{\#}$ when K-604 was administered on d0 and d3. Control mice were not significantly different than those administered K-604 alone (3 ± 0.8% versus 0.5 ± 0.6%).

For each whole-lung scan obtained of animals in each group (Fig. 2A), 40x images (n = 10) were captured at random and analyzed using ImageJ software to assess cell infiltration (Fig. 2B), lung tissue consolidation (Fig. 2C), and epithelial thickening (Fig. 2D). ITB resulted in an increased number of nuclei per high-powered field (Fig. 2B) compared with control (230 ± 3.3* versus 183 ± 5.0), consistent with a macrophage-dominant response to ITB-induced lung injury (Venosa et al., 2021). In the presence of K-604, ITB did not result in a significant increase in the number of nuclei (195 ± 7.9*). ITB resulted in consolidation of the lung tissue (Fig. 2C) as indicated by a significant decrease in white space (%) compared with control (57 ± 0.5%* versus 70 ± 0.6%). K-604 did not significantly reduce loss of white space when compared with control (62 ± 1.5%). ITB significantly increased the

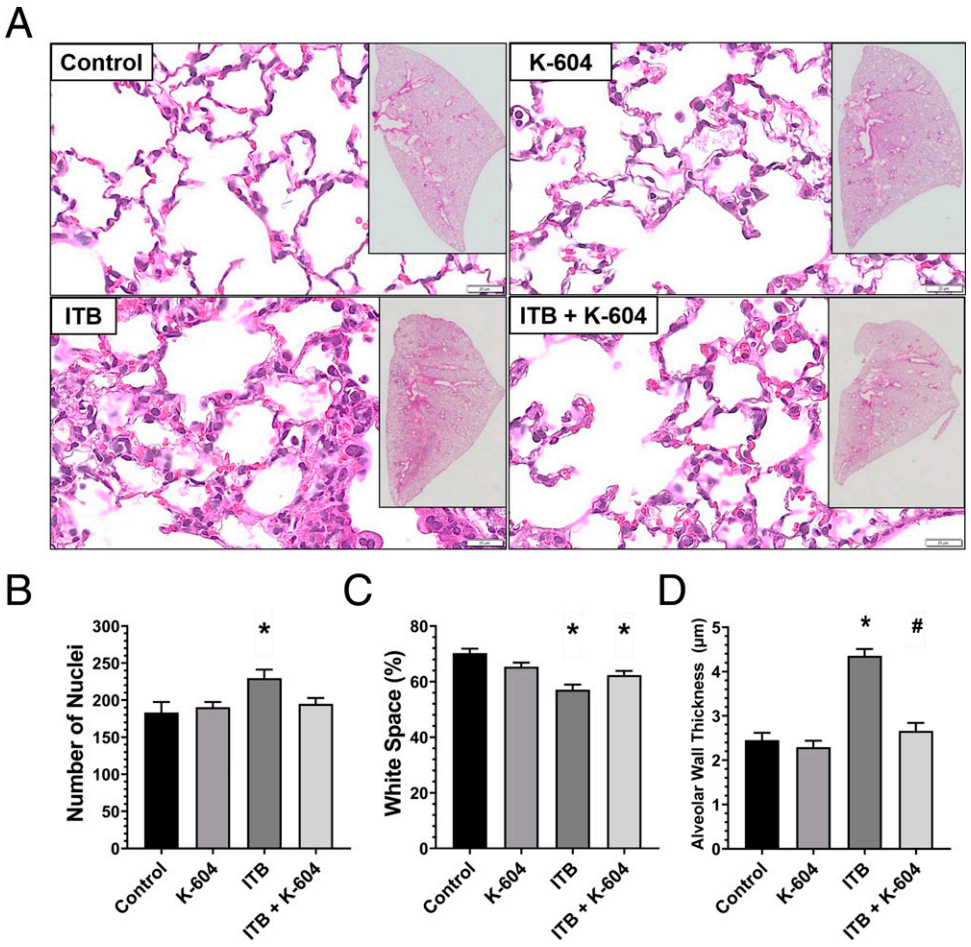

Fig. 2. Effect of K-604 on histologic markers of ITB-mediated injury. (A) Representative H&E-stained lung tissue sections derived from control (top left), K-604 (bottom left), ITB (top right) and ITB + K-604 (bottom right) treated animals (n = 16–21 per group). Images were obtained using a VS120 microscope (inset: 40x; magnified image: 400x). Randomly distributed images (n = 10) from each tissue preparation were analyzed for the number of nuclei present (B), percentage of white space (C), and average alveolar wall thickness (D). Values are expressed as mean ± standard error of the mean. (*) represents significantly different from control ($P < 0.05$); (#) represents significantly different from ITB ($P < 0.05$).

measured alveolar wall thickness (Fig. 2D) compared with control (4 ± 0.0* μm versus 2 ± 0.1 μm), which was significantly reduced by K-604 (3 ± 0.1 μm$^{\#}$).

3.2 K-604 does not Reduce ITB-Induced Epithelial Injury but Normalizes Lung Lining. ITB mediates ALI by inducing redox cycling and damage within epithelial cells (Allawzi et al., 2019), as such loss of barrier function and the accumulation of edema and protein within the BAL are hallmarks of injury. ITB increased BAL protein concentration compared with control (Fig. 3A) (2.9 ± 0.23* mg/ml versus 0.1 ± 0.19 mg/ml), which was not mitigated by K-604 administration (3.1 ± 0.21 mg/ml) indicating that K-604 did not alter the initiating injury event (ITB administration). Phospholipids within the BAL were also quantitated (Fig. 3B). ITB resulted in an increase in BAL phospholipids compared with control (117 ± 14.7 μg/30 μl* versus 23 ± 5.7 μg/30 μl) which is only partially reduced by K-604 administration (87±9.6 μg/30 μl). SP-D and SP-B concentrations were determined through western blot of the small and large phospholipid aggregate fraction, respectively (Fig. 3C). The SP-D to SP-B ratio was increased with ITB compared with control (5 ± 0.6 arbitrary units [A.U.]* versus 0.6 ± 0.2 A.U.) consistent with inflammatory activation, while an apparent decrease was observed with K-604 administration (3.0 ± 0.5*). Phospholipid levels were compared with SP-B protein levels as this ratio is critical to surfactant function (Fig. 3D). The phospholipid to SP-B ratio was increased with ITB compared with control (13 ± 2.2 A.U.* versus 1 ± 0.4 A.U). This ratio was significantly decreased in ITB + K-604 compared with ITB alone (8 ± 1.2 A.U.$^{\#}$), indicating a normalization of surface-active function.

3.3 Intratracheal K-604 Administration Mitigates ITB-Induced Cholesterol Accumulation in BAL Cells. ITB resulted in significant increases in cholesterol accumulation in BAL cells for 7 days (Fig. 4). Per 1 × 10^4 cells, total cholesterol (84 ± 13.3 μM* versus 28 ± 13.2 μM) and free cholesterol (73 ± 11.7 μM* versus 16 ± 9.1 μM) were increased in BAL cells compared with control. K-604 administration in ITB significantly reduced total cholesterol (17 ± 5.7 μM$^{\#}$), free cholesterol (14 ± 5.4 μM$^{\#}$), and cholesterol esters (7 ± 1.2 μM$^{\#}$) compared with ITB alone. These results indicate that intratracheal administration of K-604 reduces ITB-mediated increases in intracellular cholesterol and storage, as an effective dose of K-604 was delivered to inhibit Acat-1 in the lung. In alignment with increased cholesterol ester measurements with ITB, cells from ITB animals had increased cell diameter compared with control (30 ± 11.6 μm* versus 11 ± 4.3 μm), which was reduced by K-604 (14 ± 3.7 μm$^{\#}$).

To test whether transporters were involved in the observed changes in cholesterol levels, expression of cholesterol efflux transporters *Abca1* and *Abcg1* was measured in BAL cells. *Abca1* expression was not changed with ITB (1.5 ± 0.1 versus 1.1 ± 0.1), but expression was reduced in ITB + K-604 (0.44 ± 0.05$^{\#}$). *Abcg1* expression was decreased with ITB regardless of K-604 treatment compared with control (0.65 ± 0.04*, 0.61 ±

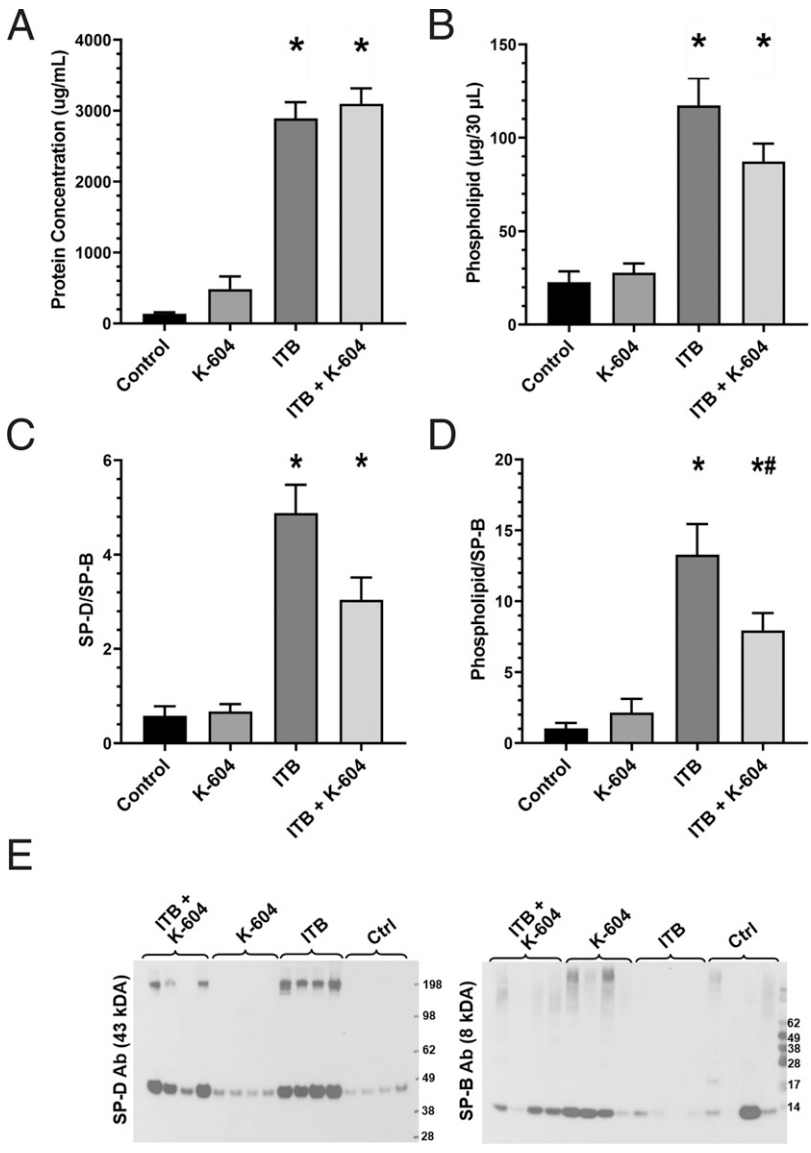

Fig. 3. Effects of ITB on total protein, phospholipid and surfactant protein expression within the BAL. Protein concentration (A), phospholipid concentration (B), SP-D:SP-B ratio (C) and phospholipid:SP-B ratio were reported (D) accompanied by representative western blots (E) from analysis of BAL fluid. Values are expressed as mean ± standard error of the mean (n = 8-12 per group). (*) represents significantly different from control ($P < 0.05$); (#) represents significantly different from ITB
($P < 0.05$).

0.05* versus 1.08 ± 0.1). These minimal changes in efflux transporter expression support that the changes in intracellular cholesterol accumulation and cell size are due to effective Acat-1 inhibition in the lung.

3.4 K-604 Treatment Reduces Alveolar and Interstitial Macrophage Activation in Response to ITB. To analyze alveolar macrophage activation, we examined BAL cells by flow cytometry using cell surface markers (Table 1). Alveolar macrophages were identified by expression of CD45, F4/80, and Siglec F (Supplemental Fig. 1). Alveolar macrophages were further categorized as mature (CD11c+/CD11b-), migratory (CD11c+/CD11b+), or recruited (CD11c-/CD11b+) (Fig. 5), where the mature population may be considered tissue-resident, and the migratory and recruited populations may be derived from the circulation or from resident cells taking on a more migratory-like phenotype. A significant loss of the mature alveolar macrophages was observed as a result of ITB administration (18 ± 4.1%* versus 95 ± 0.67%) This ITB-mediated decrease was reduced by K-604 (48 ± 6.0%$^{\#}$). ITB-induced increases in the migratory (24 ± 4.9%* versus 3 ± 0.9%) and recruited (10 ± 2.7%* versus 0.2 ± 0.1%) alveolar macrophage populations were also observed compared with control. K-604 rescued ITB-mediated increases in migratory macrophages (12 ± 2%*) but did not significantly alter the percentage of recruited macrophages (8 ± 2.0%). Alveolar macrophages were also analyzed for expression of the activation markers Ly6c and CD206. CD206 was only observed within mature alveolar macrophages and was not seen in cells that expressed Ly6c. Ly6c expression was observed in both migratory and recruited macrophages irrespective of treatment. A significant increase in pro-inflammatory (Ly6c+/CD206-) alveolar macrophages was observed following ITB-treatment compared with control (21±5.7%* versus 0.5 ± 0.2%). This increase was mitigated by K-604 administration (13 ± 4.0%$^{\#}$) indicating reduced acute macrophage activation post-ITB.

Within the lung digest, interstitial macrophages were identified by expression of CD45, F4/80, CD11b and the absence of Siglec F (Supplemental Fig. 2). The yield of interstitial macrophages was consistent across all groups. However, the percentage of cells expressing marker of maturation (CD11c and CD206) was significantly increased by ITB compared with control (Fig. 6) (20 ± 1.9%* versus 10 ± 1.5%). Administration of

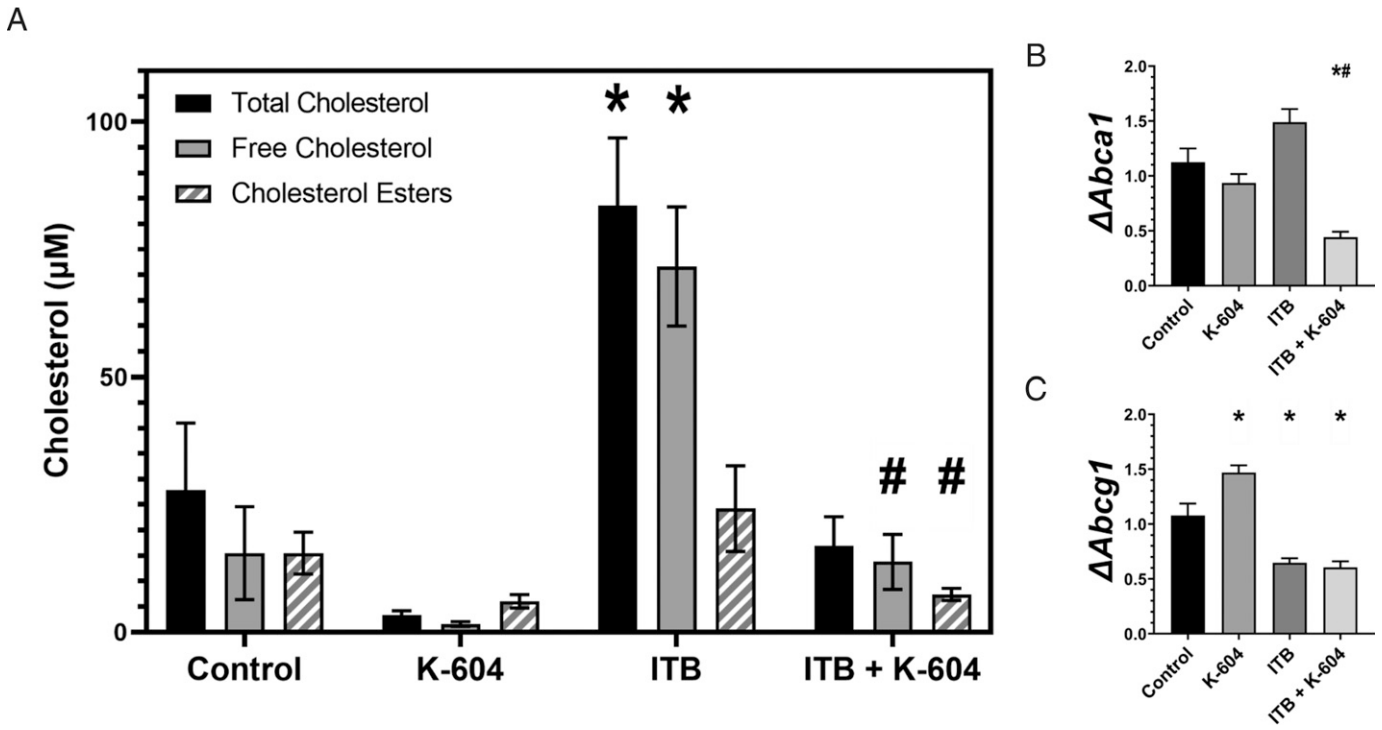

Fig. 4. K-604 reduces ITB-mediated increases cholesterol content of BAL cells. Cells from the BAL were analyzed for total cholesterol, free cholesterol, and cholesterol esters (A) reported as cholesterol (μM) per 1×10^4 cells. BAL cell expression of *Abca1* (B) and *Abcg1* (C) was determined by RT-qPCR and is shown as fold change over control. Values are expressed as mean ± standard error of the mean (n = 5–16 per group). (*) represents significantly different from control ($P < 0.05$); (#) represents significantly different from ITB ($P < 0.05$).

K-604 with ITB significantly reduced the percentage of CD11c+/CD206+ interstitial macrophages compared with ITB alone (6 ± 2.2%).

Both acute and chronic activation of macrophages have been shown to increase the expression of inducible nitric oxide synthase (*Nos2*) and arginase (*Arg1*) (MacMicking et al., 1997; Shearer et al., 1997; Kobayashi, 2010). ITB significantly increased *Nos2* (Fig. 7A) (fold change 13.5 ± 1.8* versus 1.5 ± 0.5) and *Arg1* (Fig. 7B) (fold change 239.5 ± 70* versus 2.3 ± 1.2) mRNA in BAL cells. In ITB, both *Nos2* (5.9 ± 2.0$^{\#}$) and *Arg1* (57.2 ± 11.0$^{\#}$) expression was decreased with K-604 compared with ITB alone.

TABLE 1
Expression profile of surface markers used for flow cytometric analysis of alveolar and interstitial macrophages

Cell Surface Marker	Expression Profile
CD45	Myeloid-derived cells, including alveolar and interstitial macrophages (Trowbridge and Thomas, 1994; Roach et al., 1997; Misharin et al., 2013)
Siglec F	Highly expressed on alveolar macrophages (Misharin et al., 2013; Hussell and Bell, 2014)
F4/80	Pulmonary macrophages, including alveolar and interstitial macrophages (Gordon et al., 2011; Misharin et al., 2013; Hussell and Bell, 2014)
CD11b	Indicative of a migratory phenotype; expressed on interstitial macrophages, with low expression in resident alveolar macrophages (Zaynagetdinov et al., 2013; Hussell and Bell, 2014)
CD11c	Resident alveolar macrophages and mature interstitial macrophages (Hussell and Bell, 2014)
CD206	Pro-fibrotic marker on activated interstitial macrophages. Expression on alveolar macrophages indicates an anti-inflammatory bias (Zaynagetdinov et al., 2013; Hussell and Bell, 2014; Ji et al., 2014)

4. Discussion

Herein, we show an increase in cholesterol within macrophages in response to bleomycin which is the first demonstration of such an accumulation in this model of acute lung injury. Further, we have shown that use of an Acat-1 inhibitor reduces ITB-mediated lung inflammation and macrophage activation. Using intratracheal delivery of K-604, we observed preservation of body weight, improved lung structure, and normalization of lung surfactant (Figs. 1–3). In addition, while ITB increased total, free, and cholesterol ester content in alveolar macrophages, K-604 reduced this accumulation (Fig. 4). K-604 also reduced the loss of mature alveolar macrophages (Fig. 5) and macrophage activation in both the lung lining and the interstitium (Figs. 5–7). That K-604 reduces total cholesterol and lessens injury is evidence that lipid accumulation is a significant factor within ALI.

K-604 is a known inhibitor of the enzyme Acat-1, and is highly selective for this particular acyltransferase (Shibuya et al., 2018). Acat-1 is responsible for the esterification of cholesterol to cholesterol ester, and is thus critical to lipid droplet formation (Chang et al., 2001; Chang et al., 2009). Therefore, we have used cholesterol ester as our primary endpoint to determine a sufficient level of pharmacological inhibition of Acat-1 (Fig. 4). Changes to free cholesterol, not simply cholesterol ester accumulation alone, may play a role in lipid-mediated signaling in these cells. The effects of K-604 may not be limited to cholesterol ester accumulation, as lipid-signaling pathways are complex and highly integrated. Additional work is needed

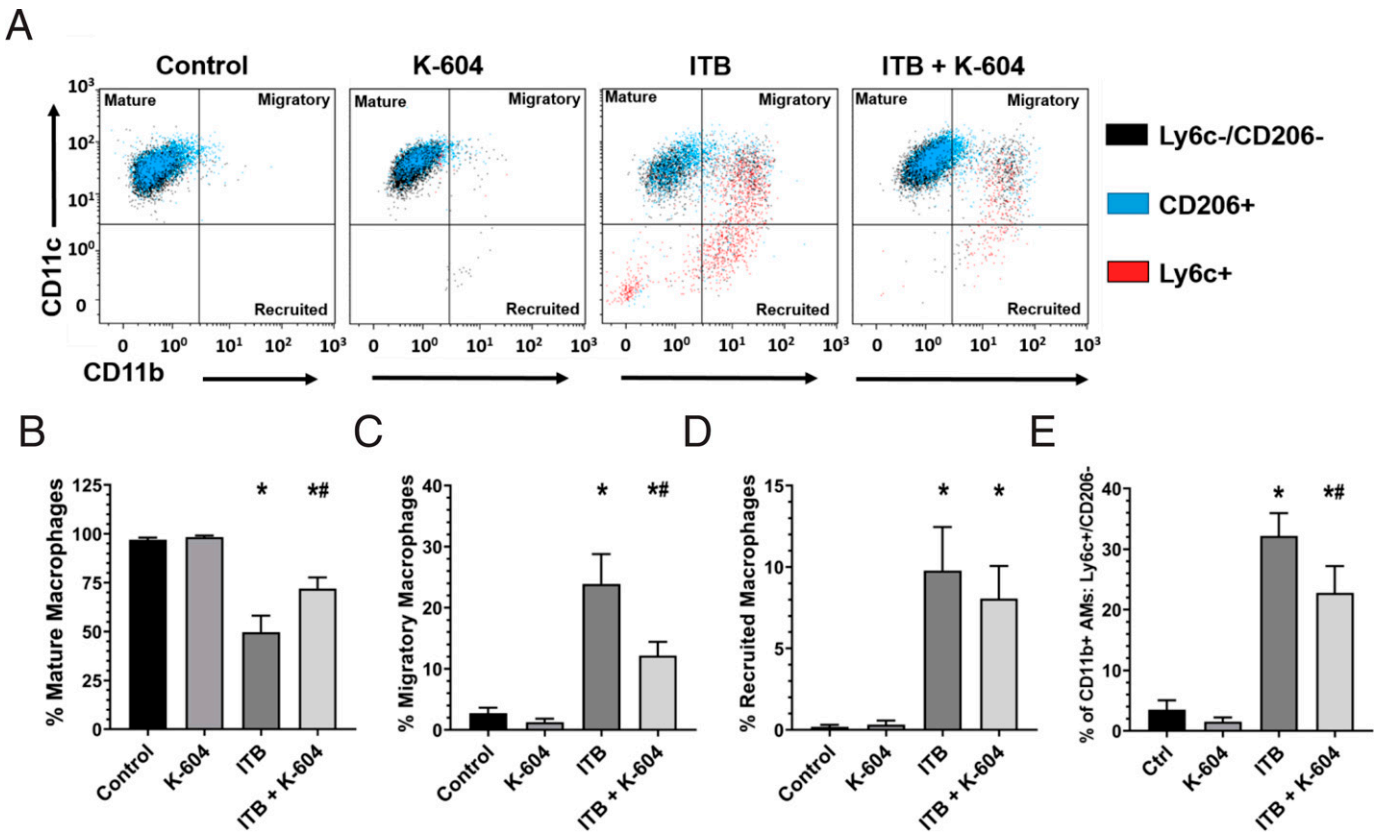

Fig. 5. Flow cytometric analysis of macrophages in the BAL fluid. Cells were immunostained and analyzed by flow cytometry (Supplemental Fig. 1). Cells that were positively stained for both Siglec F and F4/80 were determined to be alveolar macrophages (AMs). Mature macrophages (CD11c+/CD11b-), migratory macrophages (CD11c+/CD11b+), and recruited macrophages (CD11c-/CD11b+) were identified from alveolar macrophages in the BAL (A). The percentage of mature (B), migratory (C), and recruited macrophages (D) was calculated from the total number of alveolar macrophages and were assessed for their Ly6c and CD206 expression. The percentage of CD11b+ alveolar macrophages that were identified as expressing the acutely activated phenotype (Ly6c+/CD206-) was determined (E). Values are expressed as mean ± standard error of the mean (n = 8-13 per group). (*) represents significantly different from control ($P < 0.05$); (#) represents significantly different from ITB ($P < 0.05$).

to parse out downstream signaling consequences of inhibiting cholesterol esterification in these cells.

As shown previously (Chen et al., 2001; Genovese et al., 2005; Wilkinson et al., 2020), ITB resulted in a significant loss of body weight (Fig. 1). ITB-induced ALI results in increases in infiltrating macrophages, epithelial thickening, and proteinaceous debris deposition in the lung (Lindenschmidt et al., 1986; Izbicki et al., 2002; Ji et al., 2014). We observed significant increases in these criteria (Figs. 2 and 3) in response to ITB. Acat-1 inhibition with K-604 reduced body weight loss, epithelial thickening, and cellular invasion; however, it did not significantly alter BAL protein. This is consistent with K-604 reducing the inflammatory response to ITB, but not the direct epithelial injury.

The lung lining is a lipid-rich environment and the production and recycling of lipid is critical to surfactant function and homeostasis. Both alveolar type II cells and macrophages are critical in maintaining surfactant (Crouch and Wright, 2001; Weaver and Conkright, 2001; Guo et al., 2019). While type II cells produce and recycle surfactant, macrophages are responsible for its degradation (Poelma et al., 2002). SP-B and SP-C, produced by type II cells, are critical to the active regulation of surface tension (Clark et al., 1995; Stahlman et al., 2000; Weaver and Conkright, 2001; Agassandian and Mallampalli, 2013). The ratio of phospholipid:SP-B is thus an indicator of normal surfactant function. ITB increased BAL phospholipid while reducing relative SP-B expression, indicating a loss of surface-active function. K-604 restores SP-B expression, which may normalize function.

SP-D is important in innate immune regulation (Crouch and Wright, 2001; Agassandian and Mallampalli, 2013), producing both pro- and anti-inflammatory effects (Agassandian and Mallampalli, 2013). SP-D is exported via a separate vesicular pathway to SP-B by type II cells and its production favors immune regulation over surface-activity. ITB resulted in a favoring of SP-D production relative to SP-B (Fig. 3C). This SP-D:SP-B ratio was reduced by the addition of K-604 to ITB, which is consistent with a reduced inflammatory response. Also, the reduction in oxidative cross linking of SP-D in the ITB + K-604 BAL (Fig. 3E) may be indicative of a reduction in oxidative stress. Furthermore, K-604 increases SP-B levels in the BAL irrespective of ITB (Fig. 3E), indicating a bias toward surfactant production. A limitation of this study is that intratracheal administration of K-604 targets not only macrophages, but can affect all pulmonary cell types expressing Acat-1. Although macrophages highly express Acat-1, type II cells also express it (Sakashita et al., 2000). Therefore, these changes in lung lining composition may involve type II cells.

Here, we see that 7d after ITB administration, there is both cholesterol and cholesterol ester accumulation in BAL cells (Fig. 4), which is consistent with foam cell formation and persistent activation (Venosa et al., 2019). Foam cells have been

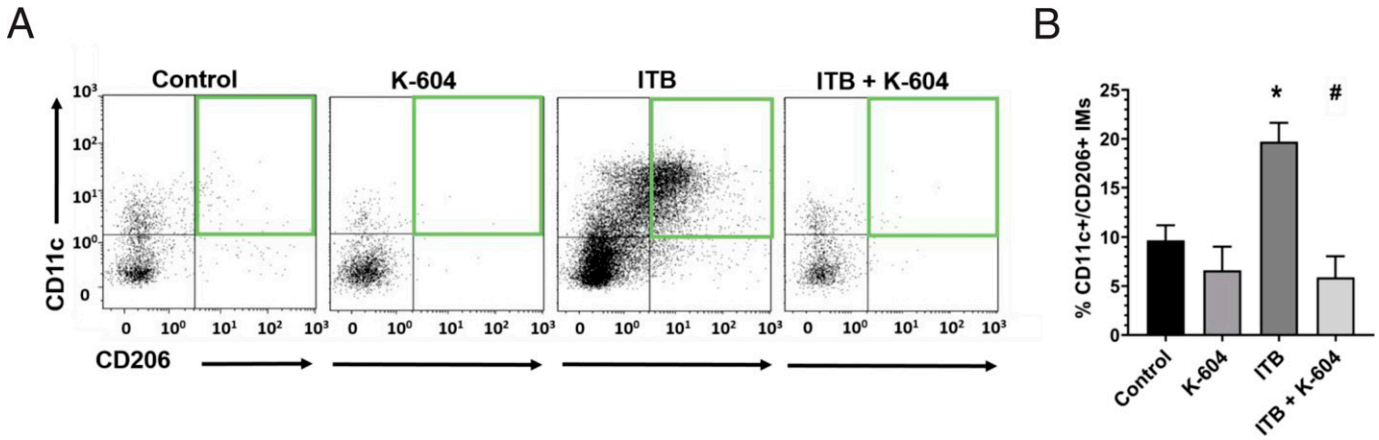

Fig. 6. Flow cytometric analysis of macrophages isolated from lung tissue. Cells from digested lung tissue were immunomagnetically-separated based upon CD45 expression. CD45+ cells were isolated, immunostained, and analyzed (Supplemental Fig 2). Cells that expressed F4/80 and CD11b in the absence of Siglec F were categorized as interstitial macrophages and were analyzed for CD11c/CD206 expression (A). The percentage of mature, chronically activated cells (CD11c+/CD206+, green box) was calculated from the total number of interstitial macrophages (B). Values are expressed as mean ± standard error of the mean (n = 8-13 per group). (*) represents significantly different from control ($P < 0.05$); (#) represents significantly different from ITB ($P < 0.05$).

well characterized in models of atherosclerosis and models of lung injury (Venosa et al., 2019), but we cannot confirm their presence in this model simply by measures of cholesterol ester accumulation. The pulmonary microenvironment, even during injury, differs greatly from that of the atherosclerotic plaque, which is known to be mediated by foam cells (Javadifar et al., 2021). In this model, while cholesterol ester accumulation is increased with ITB and reduced by K-604, one cannot conclude that these changes are associated with foam cell formation.

K-604 administration reduces cholesterol ester accumulation, indicating successful inhibition of Acat-1 in the lung. Cholesterol esterification in macrophages has previously been identified as a pharmacological target (Chinetti-Gbaguidi et al., 2015; Bouhlel et al., 2007; Yang et al., 2020) and the inhibition of Acat-1 reduces lipid-laden cell formation (Ikenoya et al., 2007). Systemic Acat-1 inhibition for the treatment of atherosclerosis, however, resulted in adverse cardiac events, halting the advancement of Acat-1 inhibitors in the clinic (Meuwese et al., 2009). To bypass potential adverse effects linked to systemic administration, we have used intratracheal instillation of K-604, which resulted in inhibition of cholesterol esterification in BAL cells without a significant increase in cell death.

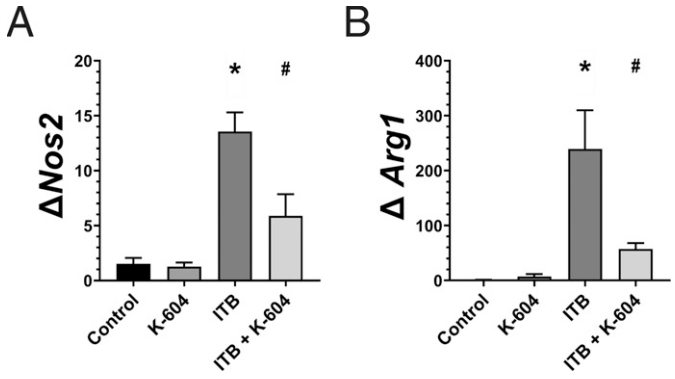

Fig. 7. K-604 inhibits ITB-mediated induction of the inflammatory enzymes *Nos2* and *Arg1*. BAL cells were analyzed for *Nos2* and *Arg1* expression by RT-qPCR. $2^{-\Delta\Delta ct}$ values were calculated using *Gapdh* as the control gene and PBS as the control condition to calculate fold change in expression. Values are expressed as mean ± standard error of the mean (n = 8 per group). (*) represents significantly different from control ($P < 0.05$); (#) represents significantly different from ITB ($P < 0.05$).

Previously, we have shown that nitrogen mustard exposure downregulates the ligand-activated liver X receptor (LXR) (Venosa et al., 2019) and its targets, the efflux transporters *Abca1* and *Abcg1* (Tontonoz and Mangelsdorf, 2003; Beyea et al., 2007), as well as reducing Acat-1 expression. In ITB alone and ITB + K-604, *Abcg1* expression was significantly decreased compared with control (Fig. 4C), highlighting that there may be a potential disruption in LXR signaling with ITB that is not rescued by K-604 administration. Although these changes are small, this may be a result of lipid-laden macrophages only being a fraction of the total BAL cell population. Regardless, additional investigation into LXR signaling and its role in lipid-laden cell formation in the context of ALI is needed. However, the changes in efflux transporter expression are insufficient to explain the lipid accumulation seen in BAL cells with ITB.

Altering lipid accumulation within macrophages can significantly alter inflammatory phenotype and indeed both alveolar and interstitial macrophage populations were shifted in response to ITB (Figs. 5 and 6). There was a significant loss of mature alveolar macrophages in response to ITB (Fig. 5B), cells that are important in the maintenance of lung homeostasis (Hussell and Bell, 2014). This population was preserved by K-604, which is consistent with reducing the post-injury inflammation. Alveolar macrophages play an essential role in surfactant recycling (Weaver and Conkright, 2001; Laskin et al., 2019), and preservation of this population may mediate the K-604-dependent improvement in surfactant homeostasis.

Macrophages are recruited to the lung lining in response to injury (Golden et al., 2022). Here, this response was blunted with K-604, as evidenced by reduced migratory macrophages in the BAL (Fig. 5C) and lowered activation (Fig. 5E). Phenotypic changes were also observed in interstitial macrophages, where mature activated macrophages were increased in response to ITB (Fig. 6B), possibly as a mechanism to replace the diminished mature alveolar macrophage population in the lung (Fig. 5). CD206+ interstitial macrophages are immunoregulatory in nature (Bedoret et al., 2009), producing cytokines that promote cell growth and differentiation as well as

favoring repair and wound healing (Schyns et al., 2019), and therefore may be pro-fibrotic. Chronic immune cell activation alters tissue composition by collagen deposition and can lead to fibrosis (Klingberg et al., 2013) and negatively impact lung function (Klingberg et al., 2013; Martinez et al., 2017). In this regard, it is significant that this CD11c+/CD206+ population of cells is reduced by K-604, suggesting Acat-1 inhibition can improve resolution and reduce fibrosis. It will be important to study these changes following ITB and K-604 treatment at time points longer than 7 days.

Arginine metabolism is critical to macrophage activation, with *Nos2* and *Arg1* expression characterizing acute and chronic activation (Rath et al., 2014; Orecchioni et al., 2019). Both *Nos2* and *Arg1* expression were significantly increased in BAL macrophages from ITB animals (Fig. 7, A and B), a response that was inhibited by K-604. K-604 therefore reduces activation without bias toward either *Nos2* or *Arg1*, implying that Acat-1 inhibition reduces both acute and chronic macrophage activation.

In conclusion, in the ITB-mediated ALI model, macrophages experience a lipid-rich extracellular environment due to direct epithelial damage, creating a biologic scenario in which there may be increased cholesterol and lipid accumulation. Macrophages in our model become large and display characteristics of the acutely-activated phenotype, which was mitigated by the intratracheal administration of an Acat-1 inhibitor. In addition to reducing cholesterol esterification, K-604 reduces the inflammatory effects of ITB-mediated lung inflammation, resulting in preservation of mature alveolar macrophages, reduced recruited and interstitial cell activation, normalization of surfactant alterations, and reduced injury. Acat-1 thus presents a potential pharmacological target in ALI; however, further investigations into the mechanisms underlying the effects of Acat-1 inhibition are necessary.

Authorship Contributions

Participated in research design: Stevenson, Guo, Gow.

Conducted experiments: Stevenson, Wilkinson, Abramova, Guo.

Performed data analysis: Stevenson, Wilkinson, Abramova, Guo.

Wrote or contributed to the writing of the manuscript: Stevenson, Gow.

References

Agassandian M and Mallampalli RK (2013) Surfactant phospholipid metabolism. *Biochim Biophys Acta* **1831**:612–625.

Allawzi A, Elajaili H, Redente EF, and Nozik-Grayck E (2019) Oxidative Toxicology of Bleomycin: Role of the Extracellular Redox Environment. *Curr Opin Toxicol* **13**:68–73.

Barbayianni I, Ninou I, Tzouvelekis A, and Aidinis V (2018) Bleomycin Revisited: A Direct Comparison of the Intratracheal Micro-Spraying and the Oropharyngeal Aspiration Routes of Bleomycin Administration in Mice. *Front Med* **5**:269.

Bartlett GR (1959) Phosphorus assay in column chromatography. *J Biol Chem* **234**:466–468.

Bedoret D, Wallemaq H, Marichal T, Desmet CJ, Calvo FQ, Henry E, Closset R Dewals B, Thielen C, Pascal G et al. Lung interstitial macrophages alter dendritic cell functions to prevent airway allergy in mice. *J Clin Invest* **119**:3723–3738.

Benoit M, Desnues B, and Mege JL (2008) Macrophage polarization in bacterial infections. *J Immunol* **181**:3733–3739.

Beyea MM, Heslop CL, Sawyez CG, Edwards JY, Markle JG, Hegele RA, and Huff MW (2007) Selective up-regulation of LXR-regulated genes ABCA1, ABCG1, and APOE in macrophages through increased endogenous synthesis of 24(S),25-epoxycholesterol. *J Biol Chem* **282**:5207–5216.

Bligh EG and Dyer WJ (1959) A rapid method of total lipid extraction and purification. *Can J Biochem Physiol* **37**:911–917.

Bouhlel MA, Derudas B, Rigamonti E, Dièvart R, Brozek J, Haulon S, Zawadzki C, Jude B, Torpier G, Marx N et al. (2007) PPARgamma activation primes human monocytes into alternative M2 macrophages with anti-inflammatory properties. *Cell Metab* **6**:137–143.

Butt Y, Kurdowska A, and Allen TC (2016) Acute Lung Injury: A Clinical and Molecular Review. *Arch Pathol Lab Med* **140**:345–350.

Chang CC, Huh HY, Cadigan KM, and Chang TY (1993) Molecular cloning and functional expression of human acyl-coenzyme A:cholesterol acyltransferase cDNA in mutant Chinese hamster ovary cells. *J Biol Chem* **268**:20747–20755.

Chang T-Y, Li B-L, Chang CCY, and Urano Y (2009) Acyl-coenzyme A:cholesterol acyltransferases. *Am J Physiol Endocrinol Metab* **297**:E1–E9.

Chang TY, Chang CC, Lin S, Yu C, Li BL, and Miyazaki A (2001) Roles of acyl-coenzyme A:cholesterol acyltransferase-1 and -2. *Curr Opin Lipidol* **12**:289–296.

Chen ES, Greenlee BM, Wills-Karp M, and Moller DR (2001) Attenuation of lung inflammation and fibrosis in interferon-gamma-deficient mice after intratracheal bleomycin. *Am J Respir Cell Mol Biol* **24**:545–555.

Chen X, Tang J, Shuai W, Meng J, Feng J, and Han Z (2020) Macrophage polarization and its role in the pathogenesis of acute lung injury/acute respiratory distress syndrome. *Inflamm Res* **69**:883–895.

Chinetti-Gbaguidi G, Colin S, and Staels B (2015) Macrophage subsets in atherosclerosis. *Nat Rev Cardiol* **12**:10–17.

Chistiakov DA, Bobryshev YV, and Orekhov AN (2016) Macrophage-mediated cholesterol handling in atherosclerosis. *J Cell Mol Med* **20**:17–28.

Chistiakov DA, Melnichenko AA, Myasoedova VA, Grechko AV, and Orekhov AN (2017) Mechanisms of foam cell formation in atherosclerosis. *J Mol Med (Berl)* **95**:1153–1165.

Clark JC, Wert SE, Bachurski CJ, Stahlman MT, Stripp BR, Weaver TE, and Whitsett JA (1995) Targeted disruption of the surfactant protein B gene disrupts surfactant homeostasis, causing respiratory failure in newborn mice. *Proc Natl Acad Sci USA* **92**:7794–7798.

Cortés I, Peñuelas O, and Esteban A (2012) Acute respiratory distress syndrome: evaluation and management. *Minerva Anestesiol* **78**:343–357.

Cross LJM and Matthay MA (2011) Biomarkers in acute lung injury: insights into the pathogenesis of acute lung injury. *Crit Care Clin* **27**:355–377.

Crouch E and Wright JR (2001) Surfactant proteins a and d and pulmonary host defense. *Annu Rev Physiol* **63**:521–554.

Dushianthan A, Grocott MP, Postle AD, and Cusack R (2011) Acute respiratory distress syndrome and acute lung injury. *Postgrad Med J* **87**:612–622.

Genovese T, Cuzzocrea S, Di Paola R, Mazzon E, Mastruzzo C, Catalano P, Sortino M, Crimi N, Caputi AP, Thiemermann C et al. (2005) Effect of rosiglitazone and 15-deoxy-Delta12,14-prostaglandin J2 on bleomycin-induced lung injury. *Eur Respir J* **25**:225–234.

Golden TN, Venosa A, and Gow AJ (2022) Cell Origin and iNOS Function Are Critical to Macrophage Activation Following Acute Lung Injury. *Front Pharmacol* **12**:761496.

Gordon S, Hamann J, Lin HH, and Stacey M (2011) F4/80 and the related adhesion-GPCRs. *Eur J Immunol* **41**:2472–2476.

Guo B, Bai Y, Ma Y, Liu C, Wang S, Zhao R, Dong J, and Ji HL (2019) Preclinical and clinical studies of smoke-inhalation-induced acute lung injury: update on both pathogenesis and innovative therapy. *Ther Adv Respir Dis* **13**:1753466619847901.

Guo C, Atochina-Vasserman E, Abramova H, George B, Manoj V, Scott P, and Gow A (2016) Role of NOS2 in pulmonary injury and repair in response to bleomycin. *Free Radic Biol Med* **91**:293–301.

Hartl D, Tirouvanziam R, Laval J, Greene CM, Habiel D, Sharma L, Yildirim AÖ, Dela Cruz CS, and Hogaboam CM (2018) Innate Immunity of the Lung: From Basic Mechanisms to Translational Medicine. *J Innate Immun* **10**:487–501.

Huang X, Xiu H, Zhang S, and Zhang G (2018) The Role of Macrophages in the Pathogenesis of ALI/ARDS. *Mediators Inflamm* **2018**:1264913.

Hussell T and Bell TJ (2014) Alveolar macrophages: plasticity in a tissue-specific context. *Nat Rev Immunol* **14**:81–93.

Ikenoya M, Yoshinaka Y, Kobayashi H, Kawamine K, Shibuya K, Sato F, Sawanobori K, Watanabe T, and Miyazaki A (2007) A selective ACAT-1 inhibitor, K-604, suppresses fatty streak lesions in fat-fed hamsters without affecting plasma cholesterol levels. *Atherosclerosis* **191**:290–297.

Ioannidis G, Lazaridis G, Baka S, Mpoukovinas I, Karavasilis V, Lampaki S, Kioumis I, Pitsiou G, Papaiwannou A, Karavergou A et al. (2015) Barotrauma and pneumothorax. *J Thorac Dis* **7** (Suppl 1):S38–S43.

Izbicki G, Segel MJ, Christensen TG, Conner MW, and Breuer R (2002) Time course of bleomycin-induced lung fibrosis. *Int J Exp Pathol* **83**:111–119.

Javadifar A, Rastgoo S, Banach M, Jamialahmadi T, Johnston TP, and Sahebkar A (2021) Foam Cells as Therapeutic Targets in Atherosclerosis with a Focus on the Regulatory Roles of Non-Coding RNAs. *Int J Mol Sci* **22**:2529.

Ji W-J, Ma Y-Q, Zhou X, Zhang Y-D, Lu R-Y, Sun H-Y, Guo Z-Z, Zhang Z, Li Y-M, and Wei L-Q (2014) Temporal and spatial characterization of mononuclear phagocytes in circulating, lung alveolar and interstitial compartments in a mouse model of bleomycin-induced pulmonary injury. *J Immunol Methods* **403**:7–16.

Johnson ER and Matthay MA (2010) Acute lung injury: epidemiology, pathogenesis, and treatment. *J Aerosol Med Pulm Drug Deliv* **23**:243–252.

Johnston LK, Rims CR, Gill SE, McGuire JK, and Manicone AM (2012) Pulmonary macrophage subpopulations in the induction and resolution of acute lung injury. *Am J Respir Cell Mol Biol* **47**:417–426.

Klingberg F, Hinz B, and White ES (2013) The myofibroblast matrix: implications for tissue repair and fibrosis. *J Pathol* **229**:298–309.

Kobayashi Y (2010) The regulatory role of nitric oxide in proinflammatory cytokine expression during the induction and resolution of inflammation. *J Leukoc Biol* **88**:1157–1162.

Laskin DL (2009) Macrophages and inflammatory mediators in chemical toxicity: a battle of forces. *Chem Res Toxicol* **22**:1376–1385.

Laskin DL, Malaviya R, and Laskin JD (2019) Role of Macrophages in Acute Lung Injury and Chronic Fibrosis Induced by Pulmonary Toxicants. *Toxicol Sci* **168**:287–301.

Lindenschmidt RC, Tryka AF, Godfrey GA, Frome EL, and Witschi H (1986) Intratracheal versus intravenous administration of bleomycin in mice: acute effects. *Toxicol Appl Pharmacol* **85**:69–77.

MacMicking J, Xie QW, and Nathan C (1997) Nitric oxide and macrophage function. *Annu Rev Immunol* **15**:323–350.

Martin TR and Frevert CW (2005) Innate immunity in the lungs. *Proc Am Thorac Soc* **2**:403–411.
Martinez FJ, Collard HR, Pardo A, Raghu G, Richeldi L, Selman M, Swigris JJ, Taniguchi H, and Wells AU (2017) Idiopathic pulmonary fibrosis. *Nat Rev Dis Primers* **3**:17074.
Matthay MA and Zimmerman GA (2005) Acute lung injury and the acute respiratory distress syndrome: four decades of inquiry into pathogenesis and rational management. *Am J Respir Cell Mol Biol* **33**:319–327.
Meuwese MC, de Groot E, Duivenvoorden R, Trip MD, Ose L, Maritz FJ, Basart DCG, Kastelein JJP, Habib R, Davidson MH et al.; CAPTIVATE Investigators (2009) ACAT inhibition and progression of carotid atherosclerosis in patients with familial hypercholesterolemia: the CAPTIVATE randomized trial. *JAMA* **301**:1131–1139.
Misharin AV, Morales-Nebreda L, Mutlu GM, Budinger GRS, and Perlman H (2013) Flow cytometric analysis of macrophages and dendritic cell subsets in the mouse lung. *Am J Respir Cell Mol Biol* **49**:503–510.
Mokra D and Kosutova P (2015) Biomarkers in acute lung injury. *Respir Physiol Neurobiol* **209**:52–58.
Müller-Redetzky HC, Suttorp N, and Witzenrath M (2014) Dynamics of pulmonary endothelial barrier function in acute inflammation: mechanisms and therapeutic perspectives. *Cell Tissue Res* **355**:657–673.
Orecchioni M, Ghosheh Y, Pramod AB, and Ley K (2019) Macrophage Polarization: Different Gene Signatures in M1(LPS+) vs. Classically and M2(LPS-) vs. Alternatively Activated Macrophages. *Front Immunol* **10**:1084.
Patel U, Rajasingh S, Samanta S, Cao T, Dawn B, and Rajasingh J (2017) Macrophage polarization in response to epigenetic modifiers during infection and inflammation. *Drug Discov Today* **22**:186–193.
Patel VJ, Biswas Roy S, Mehta HJ, Joo M, and Sadikot RT (2018) Alternative and Natural Therapies for Acute Lung Injury and Acute Respiratory Distress Syndrome. *BioMed Res Int* **2018**:2476824.
Pittet JF, Mackersie RC, Martin TR, and Matthay MA (1997) Biological markers of acute lung injury: prognostic and pathogenetic significance. *Am J Respir Crit Care Med* **155**:1187–1205.
Poelma DLH, Zimmermann LJI, Scholten HH, Lachmann B, and van Iwaarden JF (2002) In vivo and in vitro uptake of surfactant lipids by alveolar type II cells and macrophages. *Am J Physiol Lung Cell Mol Physiol* **283**:L648–L654.
Porcheray F, Viaud S, Rimaniol AC, Léone C, Samah B, Dereuddre-Bosquet N, Dormont D, and Gras G (2005) Macrophage activation switching: an asset for the resolution of inflammation. *Clin Exp Immunol* **142**:481–489.
Rath M, Müller I, Kropf P, Closs EI, and Munder M (2014) Metabolism via Arginase or Nitric Oxide Synthase: Two Competing Arginine Pathways in Macrophages. *Front Immunol* **5**:532.
Roach T, Slater S, Koval M, White L, Cahir McFarland ED, Okumura M, Thomas M, and Brown E (1997) CD45 regulates Src family member kinase activity associated with macrophage integrin-mediated adhesion. *Curr Biol* **7**:408–417.
Ross R (1999) Atherosclerosis–an inflammatory disease. *N Engl J Med* **340**:115–126.
Sakashita N, Miyazaki A, Takeya M, Horiuchi S, Chang CC, Chang TY, and Takahashi K (2000) Localization of human acyl-coenzyme A: cholesterol acyltransferase-1 (ACAT-1) in macrophages and in various tissues. *Am J Pathol* **156**:227–236.
Schyns J, Bai Q, Ruscitti C, Radermecker C, De Schepper S, Chakarov S, Farnir F, Pirottin D, Ginhoux F, Boeckxstaens G et al. (2019) Non-classical tissue monocytes and two functionally distinct populations of interstitial macrophages populate the mouse lung. *Nat Commun* **10**:3964.
Sekiya M, Osuga J, Igarashi M, Okazaki H, and Ishibashi S (2011) The role of neutral cholesterol ester hydrolysis in macrophage foam cells. *J Atheroscler Thromb* **18**:359–364.
Shearer JD, Richards JR, Mills CD, and Caldwell MD (1997) Differential regulation of macrophage arginine metabolism: a proposed role in wound healing. *Am J Physiol* **272**:E181–E190.
Shibuya K, Kawamine K, Ozaki C, Ohgiya T, Edano T, Yoshinaka Y, and Tsunenari Y (2018) Discovery of Clinical Candidate 2-(4-(2-((1 H-Benzo[d]imidazol-2-yl)thio)ethyl)piperazin-1-yl)- N-(6-methyl-2,4-bis(methylthio)pyridin-3-yl)acetamide Hydrochloride [K-604], an Aqueous-Soluble Acyl-CoA:Cholesterol O-Acyltransferase-1 Inhibitor. *J Med Chem* **61**:10635–10650.
Stahlman MT, Gray MP, Falconieri MW, Whitsett JA, and Weaver TE (2000) Lamellar body formation in normal and surfactant protein B-deficient fetal mice. *Lab Invest* **80**:395–403.
Stöger JL, Gijbels MJJ, van der Velden S, Manca M, van der Loos CM, Biessen EAL, Daemen MJAP, Lutgens E, and de Winther MPJ (2012) Distribution of macrophage polarization markers in human atherosclerosis. *Atherosclerosis* **225**:461–468.
Tam A, Wadsworth S, Dorscheid D, Man SFP, and Sin DD (2011) The airway epithelium: more than just a structural barrier. *Ther Adv Respir Dis* **5**:255–273.
Tontonoz P and Mangelsdorf DJ (2003) Liver X receptor signaling pathways in cardiovascular disease. *Mol Endocrinol* **17**:985–993.
Trowbridge IS and Thomas ML (1994) CD45: an emerging role as a protein tyrosine phosphatase required for lymphocyte activation and development. *Annu Rev Immunol* **12**:85–116.
Venosa A, Gow JG, Taylor S, Golden TN, Murray A, Abramova E, Malaviya R, Laskin DL, and Gow AJ (2021) Myeloid cell dynamics in bleomycin-induced pulmonary injury in mice; effects of anti-TNFα antibody. *Toxicol Appl Pharmacol* **417**:115470.
Venosa A, Smith LC, Murray A, Banota T, Gow AJ, Laskin JD, and Laskin DL (2019) Regulation of Macrophage Foam Cell Formation During Nitrogen Mustard (NM)-Induced Pulmonary Fibrosis by Lung Lipids. *Toxicol Sci* **172**:344–358.
Ware LB (2006) Pathophysiology of acute lung injury and the acute respiratory distress syndrome, in *Semin Respir Crit Care Med* pp 337–349.
Weaver TE and Conkright JJ (2001) Function of surfactant proteins B and C. *Annu Rev Physiol* **63**:555–578.
Wilkinson ML, Abramova E, Guo C, Gow JG, Murray A, Koudelka A, Cechova V, Freeman BA, and Gow AJ (2020) Fatty acid nitroalkenes inhibit the inflammatory response to bleomycin-mediated lung injury. *Toxicol Appl Pharmacol* **407**:115236.
Yang S, Yuan HQ, Hao YM, Ren Z, Qu SL, Liu LS, Wei DH, Tang ZH, Zhang JF, and Jiang ZS (2020) Macrophage polarization in atherosclerosis. *Clin Chim Acta* **501**:142–146.
Yu X-H, Fu Y-C, Zhang D-W, Yin K, and Tang C-K (2013) Foam cells in atherosclerosis. *Clin Chim Acta* **424**:245–252.
Zaynagetdinov R, Sherrill TP, Kendall PL, Segal BH, Weller KP, Tighe RM, and Blackwell TS (2013) Identification of myeloid cell subsets in murine lungs using flow cytometry. *Am J Respir Cell Mol Biol* **49**:180–189.

Address correspondence to: Andrew J. Gow, Ernest Mario School of Pharmacy, Department of Pharmacology & Toxicology, Rutgers, The State University of New Jersey, 160 Frelinghuysen Road, Piscataway, NJ 08854. E-mail: gow@pharmacy.rutgers.edu